

Damping and pumping of a vortex Rossby wave in a monotonic cyclone: Critical layer stirring versus inertia–buoyancy wave emission

David A. Schecter^{a)}

Department of Earth and Planetary Sciences, Harvard University, 20 Oxford Street, Cambridge, Massachusetts 02138

Michael T. Montgomery

Department of Atmospheric Science, Colorado State University, Fort Collins, Colorado 80523

(Received 21 August 2003; accepted 8 January 2004; published online 5 April 2004)

This paper further examines the rate at which potential vorticity in the core of a monotonic cyclone becomes vertically aligned and horizontally axisymmetric. We consider the case in which symmetrization occurs by the damping of a discrete vortex Rossby (VR) wave. The damping of the VR wave is caused by its stirring of potential vorticity at a critical radius r_* , outside the core of the cyclone. The decay rate generally increases with the radial gradient of potential vorticity at r_* . Previous theories for the decay rate were based on “balance models” of the vortex dynamics. Such models filter out inertia–buoyancy (IB) oscillations, i.e., gravity waves. However, if the Rossby number is greater than unity, the core VR wave can excite a frequency-matched outward propagating IB wave, which has positive feedback. To accurately account for this radiation, we here develop a theory for the decay rate that is based on the hydrostatic primitive equations. Starting from conservation of wave activity (angular pseudomomentum), an expression for the decay rate is derived. This expression explicitly demonstrates a competition between the destabilizing influence of IB wave emission, and the stabilizing influence of potential vorticity stirring at r_* . Moreover, it shows that if the radial gradient of potential vorticity at r_* exceeds a small threshold, the VR wave will decay, and the vortex will symmetrize, even at large Rossby numbers. © 2004 American Institute of Physics. [DOI: 10.1063/1.1651485]

I. INTRODUCTION

Vortices abound in planetary flow. Familiar examples are the Gulf Stream rings, hurricanes, and the polar stratospheric vortex. Many geophysical vortices tend to become symmetric, that is, vertically aligned and circular in the horizontal plane. For example, numerical simulations indicate that the vortices of planetary turbulence symmetrize on average, although individual vortices may retain some degree of tilt and ellipticity.¹ We should also remark that symmetrization is more than a geometrical curiosity. It can, in principle, contribute to the intensification of a swirling storm, such as an incipient tropical cyclone.^{2–4}

One paradigm of symmetrization is the decay of a three-dimensional (3D) deformation wave in a nearly symmetric vortex. This paper will examine a mechanism that drives the decay of the wave, and a mechanism that frustrates the decay. We will focus on a wave in an atmospheric cyclone that has strong vertical density stratification. We will assume that the mean circular wind of the cyclone does not vary with height. In addition, we will assume that the angular velocity and potential vorticity of the cyclone decrease monotonically with radius r .

Early studies of 3D symmetrization^{4–10} assumed that the vortex motion was quasigeostrophic. The quasigeostrophic

model applies only if the Rossby and Froude numbers,

$$\text{Ro} \equiv \frac{V}{L_h f} \quad \text{and} \quad \text{Fr} \equiv \frac{V}{L_v N}, \quad (1)$$

are much less than unity.^{11,12} Here, V , L_h , and L_v are the characteristic horizontal velocity, horizontal length scale, and vertical length scale of the flow. In addition, f and N are the Coriolis parameter and the buoyancy frequency of the local atmosphere; typically, $f \ll N$.

In the quasigeostrophic approximation, the cyclone supports only one class of waves. These oscillations occur due to a finite radial gradient of potential vorticity (PV), and are here called *vortex Rossby waves*.¹³ A vortex Rossby (VR) wave is either barotropic (2D) or baroclinic (3D). Figure 1 illustrates several of both kinds. Each is excited by deforming the mean PV distribution, with a specific pair of vertical (m) and azimuthal (n) wave numbers. In time, the deformed PV structure spins about the vertical axis with a constant angular phase velocity, ω_R/n . The wave frequency ω_R generally increases with n .

In a monotonic cyclone, a VR wave is damped by a resonance with the fluid rotation at a critical radius r_* .^{9,14–20} The critical radius satisfies the equation

^{a)}Present address: Department of Atmospheric Science, Colorado State University, Fort Collins, CO 80523.

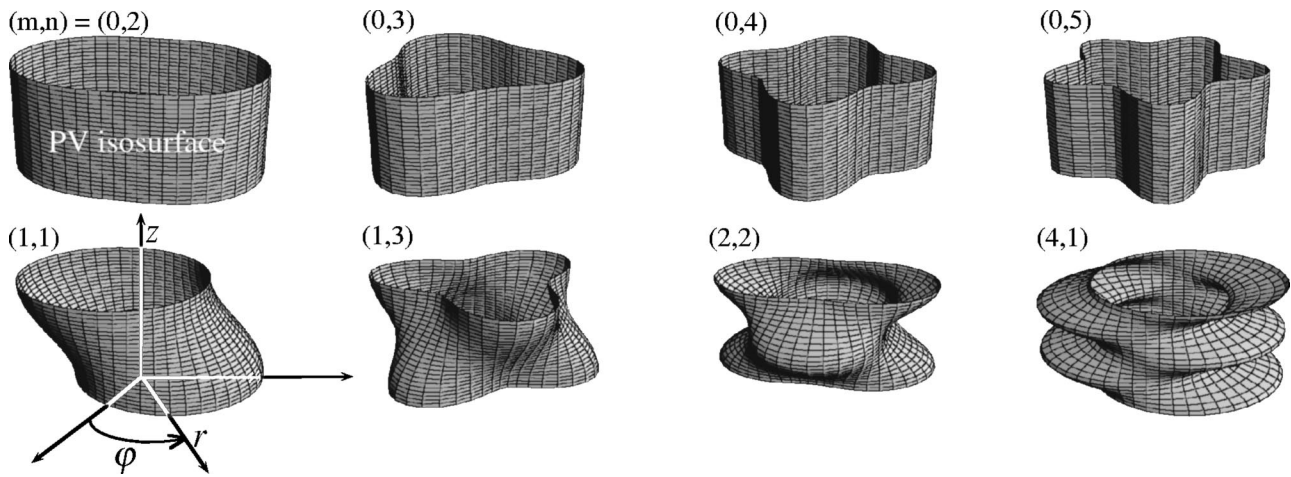


FIG. 1. Deformed PV isosurfaces corresponding to a selection of barotropic (top row) and baroclinic (bottom row) VR waves. The wave amplitudes are exaggerated for clarity.

$$\bar{\Omega}(r_*) = \omega_R/n, \tag{2}$$

in which $\bar{\Omega}(r)$ is the angular velocity of the mean cyclone. Figure 2 illustrates how cat's eyes develop in the horizontal flow near r_* , upon excitation of a VR wave ($n=2$). The perturbed flow in and near the cat's eyes efficiently redistributes PV. For a monotonic cyclone, this redistribution has negative feedback, and causes the wave to decay, exponentially at early times. The decay rate is proportional to the radial derivative of PV at r_* . We will often refer to this decay as *critical layer (CL) damping*.

A recent effort was made to extend the theory of damped VR waves to rapidly rotating cyclones, which have Rossby numbers of order unity or greater.²⁰ The analysis was based on an asymmetric balance (AB) approximation of the wave dynamics.^{21–23} Overall, the AB theory of VR waves compared well to numerical simulations, based on less approximate primitive equations. However, the accuracy of AB theory declined as the Rossby number became much greater than unity. The error arose for the following reason: at such large Rossby numbers, baroclinic VR waves can resonantly excite inertia-buoyancy (IB) oscillations in the ambient fluid. AB theory, like any balance model, neglects the creation and feedback of these oscillations.

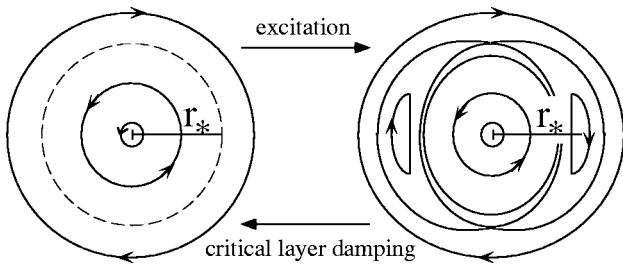


FIG. 2. Streamlines of the horizontal flow (in a rotating frame) at an arbitrary height z . The excitation of a VR wave creates cat's eyes at r_* . “Stirring” of PV in this critical layer causes the wave to decay, and the vortex to symmetrize. In this paper, we will assume that the wave amplitude is sufficiently small to avoid nonlinear arrest of the decay (see Refs. 14, 15, 18, and 19).

Figure 3 illustrates the potential error of neglecting IB waves in the environment. The contour plots show the dynamical pressure perturbation (ϕ') that is produced by a VR wave in a Rankine cyclone, with $Ro=10$. According to the primitive equations [Fig. 3(a)], the core VR wave emits a frequency-matched, spiral IB wave into the environment. It has been shown that such emission has positive feedback.^{24–30} In this example, there is effectively no PV gradient at r_* to provide negative feedback. As a result, the amplitude of the VR wave doubles in 5.6 eddy turnovers (not shown). In contrast, AB theory [Fig. 3(b)] permits no radiation, and predicts a stable wave.

In a similar way, a VR wave can amplify by emitting a sound wave.^{31,32} Since the cyclones of interest have Mach numbers much less than unity, we need not concern ourselves with acoustic destabilization. However, the following trend should be noted: VR waves tend to grow as the vortex loses energy and angular momentum to the environment, by

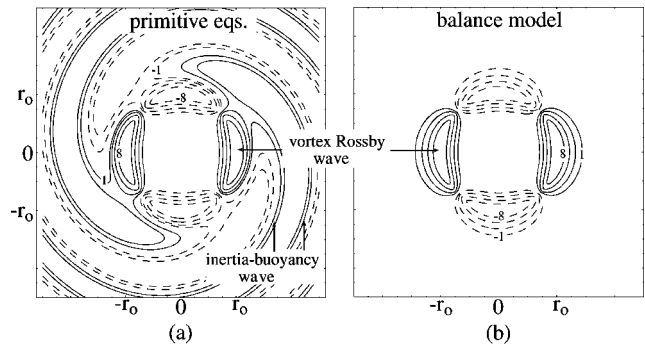


FIG. 3. Dynamical pressure perturbation (ϕ') produced by the $(m,n) = (2,2)$ VR mode of a smoothed Rankine cyclone [Eq. (37)], at an arbitrary height z , according to: (a) the primitive equations and (b) the asymmetric balance model. Solid and dashed contours indicate positive and negative anomalies. The contour levels are the same in (a) and (b) and have arbitrary units. The cyclone parameters are $Ro=10$, $l_2=r_0$, and $\Delta=0.025$. Equations (20) and (42) precisely define Ro and the deformation radius l_2 . Equation (37) defines the smoothness parameter Δ and the core radius r_0 . The Froude number, given here by $Fr=Ror_0/l_2$, is 10.

various means. This indicates that VR waves carry negative energy and negative angular momentum.¹⁴

In this paper, we will revise the theory of discrete VR waves in geophysical cyclones to incorporate *both* critical layer stirring and IB wave emission. The revised theory will be based on the linearized hydrostatic primitive equations. A growth rate formula [Eq. (70)] will be derived as a corollary to conservation of wave activity, i.e., angular pseudomomentum. This formula will clearly demonstrate the negative feedback of critical layer stirring and the positive feedback of IB wave emission. It will further show that there is a critical value of the radial PV gradient at r_* , above which the VR wave is damped, and below which the wave will grow. Balance models are justified only if the PV gradient far exceeds this critical value, and therefore dwarfs the influence of ambient IB waves (cf. Refs. 28 and 33). We will verify the revised growth rate formula upon comparison to numerics.

There are four subtle issues to address before advancing to the main text. The first issue concerns the modal classification of a VR wave. A growing VR wave appears as an exact eigenmode of the linearized perturbation equations. A damped VR wave does not; instead, it appears as a quasimode.^{8,9,14–20} Physically, a quasimode hardly differs from an eigenmode. It behaves like a single exponentially damped wave over the bulk of the vortex; however, in a thin critical layer, the PV perturbation grows.

The second issue concerns our restricted use of the term “VR wave.” In this paper, the term generally refers to a discrete mode of oscillation. However, the literature also describes sheared VR waves.^{2–4,23,34–42} Discrete and sheared VR waves differ considerably. For example, the pressure field of a sheared VR wave can decay algebraically, as opposed to exponentially, with time. Although an arbitrary PV perturbation blends discrete and sheared waves, discrete waves typically dominate vortex deformations.^{8,9,15,18,42,43}

The third issue concerns our focus on monotonic cyclones, as opposed to arbitrary vortices. In this paper, we do not discuss anticyclones, because they suffer centrifugal instabilities at large Rossby numbers.⁴⁴ We further assume monotonicity to ensure that stirring in the critical layer damps the VR wave. If the slopes of PV in the core and critical layer were opposite, stirring at r_* would ironically amplify the wave.¹⁴

The fourth issue concerns the limitations of linear theory. Although linear theory provides useful insight, there are various nonlinear processes that merit future investigation. For example, nonlinear stirring in the critical layer decreases the magnitude of the radial PV gradient at r_* .^{3,4,14,15,18,19} If the initial wave amplitude is sufficiently large, this gradient might eventually drop below the stability threshold.⁴⁵ Furthermore, finite amplitude VR waves interact with others. This may lead to beat-wave damping,⁴⁶ among other effects.

Finally, although they do not pertain directly to geophysical vortices, there are several analogous papers worth mentioning. These papers analyze waves in straight shear flow^{47–49} and in stellar accretion disks.^{50–52} In general, they discuss how PV stirring in the critical layer affects wave stability. The accretion disk papers further discuss the positive feedback of sound-wave emission (as opposed to IB

wave emission). Most notably, Papaloizou and Pringle⁵⁰ derive a growth rate formula for accretion disk waves that closely resembles our Eq. (70).

The remainder of this paper is organized as follows: Section II reviews the hydrostatic primitive equations. Section III presents the equations that govern 3D perturbations in a barotropic cyclone. Section IV describes the VR–IB wave instability in the context of linear eigenmode theory. Section V shows how the VR–IB wave instability is quenched as the radial PV gradient increases above a threshold in the critical layer. Section VI contains the main result of this paper. In it, we derive a formula for the growth rate of a VR wave, which takes into account both CL damping and IB wave emission. This formula agrees quantitatively with the growing and damped waves of Secs. IV and V. Section VII recapitulates our conclusions and discusses their possible relevance to tropical cyclone dynamics.

II. MODEL FOR ATMOSPHERIC FLOW

In this paper, we will focus on vortex dynamics in a dry, stably stratified atmosphere, for which the equation of state is approximately that of an ideal gas, $p = \rho RT$. Here, $p(\mathbf{x}, t)$ is pressure, $\rho(\mathbf{x}, t)$ is mass density, $T(\mathbf{x}, t)$ is temperature, R is the gas constant, \mathbf{x} is the position vector, and t is time. We will neglect frictional effects, thermal diffusivity, and spatial variation of the Coriolis parameter f . Finally, we will employ the hydrostatic and Boussinesq approximations. The resulting model can also apply to oceanic flow,¹¹ with an appropriate change of variables (Appendix A).

We will use the pressure-based coordinate system of Hoskins and Bretherton (HB), which is a staple of dynamical meteorology.⁵³ The HB coordinate system uses a function of pressure for the vertical coordinate, rather than the actual height variable z_* . This function, called “pseudoheight,” is defined below:

$$z(p) \equiv \left[1 - \left(\frac{p}{p_0} \right)^{R/c_p} \right] \frac{c_p}{R} \frac{p_0}{\rho_0 g}, \quad (3)$$

where g is the gravitational acceleration, c_p is the isobaric specific heat of the atmosphere, and p_0 (ρ_0) is a constant reference pressure (density).

Assuming hydrostatic balance, z increases (p decreases) monotonically with z_* . Hydrostatic balance also implies the differential relation, $dz = dz_* \theta_0 / \theta$. Here, $\theta(\mathbf{x}, t) \equiv T(p_0/p)^{R/c_p}$ is the potential temperature, and θ_0 is the reference temperature. The potential temperature relates to the specific entropy by $s = c_p \ln(\theta/\theta_0)$.

In the HB coordinate system, the equations of motion are

$$\partial_t \mathbf{u} + \mathbf{v} \cdot \nabla \mathbf{u} + f \hat{z} \times \mathbf{u} + \nabla_h \phi = 0, \quad (4)$$

$$\theta = \theta_0 \partial_z \phi / g, \quad (5)$$

$$\partial_t \theta + \mathbf{v} \cdot \nabla \theta = 0, \quad (6)$$

$$\nabla \cdot \rho_p \mathbf{v} = 0, \quad (7)$$

where $\nabla_h \equiv \hat{x} \partial_x + \hat{y} \partial_y$, and $\nabla \equiv \nabla_h + \hat{z} \partial_z$. Equation (4) is the momentum equation, describing the evolution of the horizontal velocity field $\mathbf{u}(\mathbf{x}, t)$. The 3D velocity field is given by

$\mathbf{v}(\mathbf{x}, t) = \mathbf{u} + w\hat{z}$, where $w(\mathbf{x}, t)$ is the material derivative of z . Note that the pressure force was transformed into the gradient of the geopotential, $\phi(\mathbf{x}, t) \equiv gz_*$. Equation (5) is a convenient expression of hydrostatic balance. Equation (6) is the adiabatic heat equation. Equation (7) is mass conservation. It involves the pseudodensity, defined by

$$\rho_p(z) \equiv \rho_0 \left(\frac{p}{p_0} \right)^{c_v/c_p} \tag{8}$$

In the Boussinesq approximation, ρ_p is treated as a constant in (7), and divided through on both sides to obtain

$$\nabla \cdot \mathbf{v} = 0. \tag{9}$$

Hereafter, we will use the Boussinesq approximation.

In addition to conserving entropy, our atmospheric model [Eqs. (4)–(6), (9)] conserves Boussinesq potential vorticity

$$q(\mathbf{x}, t) \equiv (\nabla \times \mathbf{u} + f\hat{z}) \cdot \nabla \theta \tag{10}$$

along material trajectories. That is,

$$\partial_t q + \mathbf{v} \cdot \nabla q = 0. \tag{11}$$

It is possible to construct additional flux-conservative equations from (4) to (6) and (9). One is for the evolution of energy density

$$\partial_t \mathcal{E} = -\nabla \cdot \mathbf{F}_e, \tag{12}$$

in which

$$\mathcal{E}(\mathbf{x}, t) \equiv \frac{\mathbf{u}^2}{2} + \phi - \phi|_{z=0}, \tag{13}$$

and

$$\mathbf{F}_e(\mathbf{x}, t) \equiv \mathbf{v} \left(\frac{\mathbf{u}^2}{2} + \phi \right) + \int_0^z dz' \mathbf{u} \partial_{z'} \phi - \hat{z} z (w \partial_z \phi)|_{z=0}. \tag{14}$$

Another is for the evolution of vertical angular momentum density

$$\partial_t \mathcal{L} = -\nabla \cdot \mathbf{F}_l, \tag{15}$$

in which

$$\mathcal{L}(\mathbf{x}, t) \equiv \hat{z} \cdot (\mathbf{x} \times \mathbf{u}), \tag{16}$$

and

$$\mathbf{F}_l(\mathbf{x}, t) \equiv \mathbf{v} \left[\hat{z} \cdot (\mathbf{x} \times \mathbf{u}) + \frac{fr^2}{2} \right] + \hat{z} \times \mathbf{x} \phi. \tag{17}$$

Note that $r^2 \equiv (\hat{z} \times \mathbf{x})^2$. Finally, we have

$$\partial_t C(q, \theta) = -\nabla \cdot \mathbf{v} C(q, \theta), \tag{18}$$

where C is an arbitrary function of potential vorticity and potential temperature. Of course, any linear combination of \mathcal{E} , \mathcal{L} , and C will also satisfy a flux-conservative equation.

The fluid dynamics is generally sensitive to the boundary conditions. We will focus on flow in a horizontal layer, bounded between $z=0$ and H . For simplicity, we will assume that θ is constant along the top ($z=H$) and bottom ($z=0$) surfaces. From Eq. (6), and the convective stability

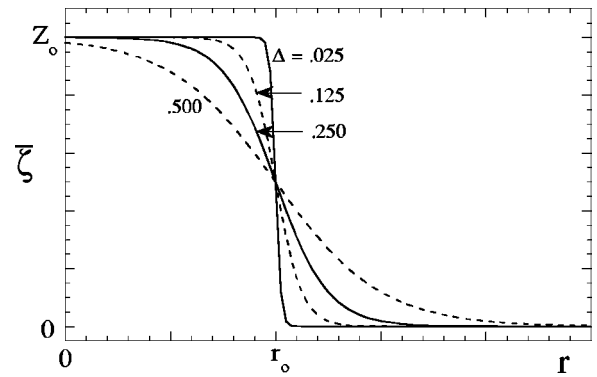


FIG. 4. The relative vorticity of a smoothed Rankine cyclone. The potential vorticity, $\bar{q} \propto f + \bar{\zeta}$, has the same form. Equation (37) defines the parameters r_0 and Δ .

condition $\partial_z \theta > 0$, constant θ implies zero vertical velocity ($w=0$). Accordingly, the vertical energy flux ($\mathbf{F}_e \cdot \hat{z}$) and vertical angular momentum flux ($\mathbf{F}_l \cdot \hat{z}$) both vanish at $z=0$ and H . However, we will allow energy and angular momentum to leave the radial boundary via waves.

III. PERTURBATIONS IN A CYCLONE

We now present the equations that govern 3D perturbations in a barotropic cyclone. In general, we will denote the perturbation of a field $\chi(\mathbf{x}, t)$ about the basic state $\bar{\chi}(r, z)$ by a prime; i.e., $\chi'(\mathbf{x}, t) \equiv \chi - \bar{\chi}$. In addition, we will use a cylindrical coordinate system (r, φ, z) (see Fig. 1), in which the vector field (u, v, w) gives the radial, azimuthal, and vertical velocities, in that order.

A. Unperturbed cyclone

The unperturbed cyclone is characterized by its azimuthal velocity profile $\bar{v}(r)$. For convenience, we define the auxiliary fields

$$\begin{aligned} \bar{\Omega}(r) &\equiv \frac{\bar{v}}{r}, & \bar{\zeta}(r) &\equiv \frac{1}{r} \frac{d(r\bar{v})}{dr}, \\ \bar{\xi}(r) &\equiv f + 2\bar{\Omega}, & \bar{\eta}(r) &\equiv f + \bar{\zeta}. \end{aligned} \tag{19}$$

Here, $\bar{\Omega}$ is the angular rotation frequency, $\bar{\zeta}$ is the vertical vorticity, $\bar{\xi}$ is the modified Coriolis parameter, and $\bar{\eta}$ is the absolute vorticity. The intensity of the cyclone is measured by the central Rossby number

$$\text{Ro} = \frac{\bar{\zeta}(0)}{f}. \tag{20}$$

Figure 4 shows the vertical vorticity $\bar{\zeta}$ for a class of cyclones that we will examine.

The unperturbed vortex is stationary due to a balance of forces. This includes gradient balance

$$\partial_r \bar{\phi} = f\bar{v} + \frac{\bar{v}^2}{r}, \tag{21}$$

and hydrostatic balance

$$\partial_z \bar{\phi} = \frac{g}{\theta_0} \bar{\theta}. \quad (22)$$

The positive derivative of $\bar{\theta}(z)$ determines the buoyancy frequency

$$N \equiv \sqrt{\frac{g}{\theta_0} \frac{d\bar{\theta}}{dz}} = \sqrt{\partial_{zz} \bar{\phi}}. \quad (23)$$

To simplify future analysis, we will assume that N is constant.

The unperturbed PV distribution is given by

$$\bar{q}(r) \equiv (f + \bar{\zeta}) \frac{d\bar{\theta}}{dz} = \frac{\theta_0 N^2}{g} (f + \bar{\zeta}). \quad (24)$$

Note that $d\bar{q}/dr$ is proportional to, and has the same sign as, $d\bar{\zeta}/dr$. Therefore, the unperturbed PV and vorticity gradients are essentially the same.

B. Linearized dynamics

The perturbation equations are easily derived from the original model (4)–(6), (9). In cylindrical coordinates, the linearized equations for the velocity and geopotential perturbations are

$$\partial_t u' + \bar{\Omega} \partial_\varphi u' - \bar{\xi} v' + \partial_r \phi' = 0, \quad (25)$$

$$\partial_t v' + \bar{\Omega} \partial_\varphi v' + \bar{\eta} u' + \frac{1}{r} \partial_\varphi \phi' = 0, \quad (26)$$

$$\partial_t \partial_z \phi' + \bar{\Omega} \partial_\varphi \partial_z \phi' + w' N^2 = 0, \quad (27)$$

$$\frac{1}{r} \partial_r (r u') + \frac{1}{r} \partial_\varphi v' + \partial_z w' = 0. \quad (28)$$

In addition, the linearized potential vorticity equation is

$$\partial_t q' + \bar{\Omega} \partial_\varphi q' + u' \frac{d\bar{q}}{dr} = 0, \quad (29)$$

in which, to first order,

$$q' = \frac{\theta_0 N^2}{g} (\nabla \times \mathbf{u}') \cdot \hat{z} + \frac{\theta_0}{g} \bar{\eta} \partial_{zz} \phi'. \quad (30)$$

C. Wave activity

To simplify future analysis of modal growth and decay, we will appeal to conservation of wave activity. The wave activity in a vortex of radius r_v is defined by

$$A_v(t; r_v) \equiv - \int_0^{2\pi} \int_0^H \int_0^{r_v} (d\varphi dz dr) \mathcal{L}_p, \quad (31)$$

in which

$$\mathcal{L}_p(r, \varphi, z, t) \equiv \frac{g}{2\theta_0 N^2} \frac{r(q')^2}{d\bar{q}/dr} + \frac{r \partial_z v' \partial_z \phi'}{N^2} \quad (32)$$

is the ‘‘angular pseudomomentum.’’ Appendix B explains how \mathcal{L}_p closely relates to the vertical angular momentum

density of a perturbation. The reader may consult Refs. 22, 23, and 54–59 for more details on angular pseudomomentum and its cousins.

The following steps lead to a flux-conservative equation for \mathcal{L}_p :

- (i) differentiate Eq. (26) with respect to z ;
- (ii) multiply the new Eq. (26) by $r \partial_z \phi' / N^2$;
- (iii) multiply Eq. (27) by $r \partial_z v' / N^2$;
- (iv) multiply Eq. (29) by

$$\frac{g}{\theta_0 N^2} \frac{r}{d\bar{q}/dr} q';$$

- (v) sum the new Eqs. (26), (27), and (29).

Simplifying the sum yields

$$\partial_t \mathcal{L}_p = -\nabla \cdot \mathbf{F}_p, \quad (33)$$

in which

$$\begin{aligned} \mathbf{F}_p \equiv & \hat{r} r u' v' \\ & + \hat{\phi} \left\{ r \bar{\Omega} \mathcal{L}_p + \frac{r}{2N^2} (\partial_z \phi')^2 + \frac{r}{2} [(v')^2 - (u')^2] \right\} \\ & + \hat{z} \left(\frac{\bar{\eta} r}{N^2} u' \partial_z \phi' + r w' v' \right). \end{aligned} \quad (34)$$

Note that the flux of angular pseudomomentum ($\mathbf{F}_p \cdot \hat{z}$) vanishes at the vertical boundaries, since $\partial_z \phi' = 0 = w'$ at $z = 0$ and at $z = H$.

The volume integral of Eq. (33) implies that

$$\frac{dA_v}{dt} = S_{\text{rad}}, \quad (35)$$

in which

$$S_{\text{rad}}(t; r_v) \equiv \int_0^{2\pi} \int_0^H (d\varphi dz) r_v^2 (u' v')_{r_v}. \quad (36)$$

Fundamentally, S_{rad} is the rate at which wave activity enters the vortex from the environment. It is also the outward flux of vertical angular momentum.

IV. INSTABILITY OF A RANKINE CYCLONE: INERTIA–BUOYANCY WAVE EMISSION

A. Smoothed Rankine cyclone

We now describe the potential instability of a rapidly rotating monotonic cyclone in greater detail. In particular, we consider a smoothed Rankine cyclone, defined by

$$\bar{\zeta}(r) = \frac{Z_0}{2} \left[1 - \tanh \left(\frac{r - r_0}{r_0 \Delta} \right) \right]. \quad (37)$$

Here, Z_0 is the central vorticity and Δ is a smoothness parameter. Figure 4 illustrates how the smoothness increases as Δ increases.

We will only consider cases in which the Rossby number $\text{Ro} = Z_0 / f$ exceeds unity. Only then can a VR wave, on the scale of the vortex, emit a frequency-matched IB wave into the environment.^{60,61} Such emission is required for instability

in an unbounded system. Balance models, which neglect IB waves, generally purport that unbounded monotonic cyclones are stable.⁶²

B. The eigenmode problem

The VR–IB wave instability appears as an exponentially growing normal mode. A normal mode of a monotonic cyclone, with isothermal boundaries at $z=0$ and $z=H$, has the form

$$\begin{aligned} \phi'(r, \varphi, z, t) &= a\Phi(r)\cos(m\pi z/H)e^{i(n\varphi - \omega t)} + \text{c.c.}, \\ u'(r, \varphi, z, t) &= aU(r)\cos(m\pi z/H)e^{i(n\varphi - \omega t)} + \text{c.c.}, \\ v'(r, \varphi, z, t) &= aV(r)\cos(m\pi z/H)e^{i(n\varphi - \omega t)} + \text{c.c.}, \\ w'(r, \varphi, z, t) &= aW(r)\sin(m\pi z/H)e^{i(n\varphi - \omega t)} + \text{c.c.}, \\ q'(r, \varphi, z, t) &= aQ(r)\cos(m\pi z/H)e^{i(n\varphi - \omega t)} + \text{c.c.}, \end{aligned} \tag{38}$$

where a is an arbitrary constant, and c.c. denotes the complex conjugate.

Substituting the normal mode solution into Eqs. (25)–(28), and performing some manipulation, we obtain

$$\begin{aligned} \frac{1}{r} \frac{d}{dr} \left[\frac{r}{\bar{\mu} - \sigma^2} \frac{d}{dr} \Phi \right] - \frac{n}{\sigma r} \frac{d}{dr} \left[\frac{\bar{\xi}}{\bar{\mu} - \sigma^2} \right] \Phi \\ - \left[\frac{n^2}{r^2(\bar{\mu} - \sigma^2)} + \frac{1}{f^2 l_m^2} \right] \Phi = 0, \end{aligned} \tag{39}$$

where

$$\bar{\mu}(r) \equiv \bar{\xi} \bar{\eta} \tag{40}$$

is the ‘‘inertial stability,’’

$$\sigma(r) \equiv \omega - n\bar{\Omega} \tag{41}$$

is the complex Doppler shifted mode frequency, and

$$l_m \equiv NH/m\pi|f| \tag{42}$$

is the m th internal Rossby deformation radius. The complex mode frequencies are the values of ω that permit a solution to Eq. (39), with prescribed radial boundary conditions.

Once a solution is found for Φ , the other field variables are obtained by the following relations:

$$\begin{aligned} U(r) &= \frac{i}{\bar{\mu} - \sigma^2} \left(\sigma \frac{d\Phi}{dr} - \frac{n\bar{\xi}}{r} \Phi \right), \\ V(r) &= \frac{1}{\bar{\mu} - \sigma^2} \left(\bar{\eta} \frac{d\Phi}{dr} - \frac{n\sigma}{r} \Phi \right), \\ W(r) &= -\frac{im\pi\sigma}{HN^2} \Phi, \\ Q(r) &= \frac{-i}{\sigma} \frac{d\bar{q}}{dr} U. \end{aligned} \tag{43}$$

In general, σ is complex, and the resonant denominators in Eqs. (43) are nonzero for all r . Appendix C analyzes the modal solution near the resonances. It turns out that the inertial resonances, where $\bar{\mu} = \sigma^2$, are spurious singularities.

In what follows, we will focus on nonaxisymmetric ($n \geq 1$) baroclinic ($m \geq 1$) modes. Other modes are either pure VR waves ($m=0$) or pure IB waves ($n=0$). Accordingly, other modes cannot represent hybrid instabilities.

To find the normal modes, we must specify the radial boundary conditions. As $r \rightarrow 0$, there exist two independent solutions to Eq. (39):

$$\begin{aligned} \Phi_I^{(1)}(r) &\sim r^{-n}, \quad n \geq 1, \\ \Phi_I^{(2)}(r) &\sim r^n, \quad n \geq 1. \end{aligned} \tag{44}$$

The singular solution $\Phi_I^{(1)}$ is rejected on physical grounds, leaving $\Phi_I^{(2)}$ as the natural choice. This implies the following mixed boundary condition at a point near the origin:

$$\frac{d\Phi}{dr} \simeq \frac{n}{r} \Phi. \tag{45}$$

As $r \rightarrow \infty$, i.e., in the radiation zone, there also exist two independent solutions to Eq. (39); they are

$$\Phi_{II}^{(1)}(r) \sim H_0^{(1)}(\kappa), \quad \Phi_{II}^{(2)}(r) \sim H_0^{(2)}(\kappa), \tag{46}$$

in which

$$\kappa \equiv \frac{\sqrt{\omega^2/f^2 - 1}}{l_m} r, \quad -\pi/2 < \arg(\kappa) \leq \pi/2, \tag{47}$$

and $H_0^{(j)}$ is the zeroth-order Hankel function of the j th kind. The associated mixed boundary conditions at a point $\kappa^2 \gg n^2$, and r much greater than the vortex scale, are

$$\frac{d\Phi}{dr} \simeq -i^{2j+1} \frac{\sqrt{\omega^2/f^2 - 1}}{l_m} \Phi. \tag{48}$$

The first ($j=1$) and second ($j=2$) Hankel functions correspond to radially outward and radially inward propagating waves (spiral if $n \geq 1$). As in related literature,⁴⁴ we will choose the outward propagating ($j=1$) wave as the ‘‘radiation condition’’ for an unbounded medium. In Appendix D, we discuss another possibility—the sponge-ring boundary condition. The sponge ring deserves some attention, because it is often used in numerical simulations.

To compute the normal modes, we generally use a center-point shooting scheme. We first obtain the inner and outer solutions of Eq. (39) for a trial value of ω . The inner solution (Φ_I) must satisfy Eq. (45) at a radius ε near zero. The outer solution (Φ_{II}) must satisfy Eq. (48) ($j=1$) at a sufficiently large radius r_b . The value of ω is varied until the Wronskian

$$\text{Wk}(\omega, r) \equiv \Phi_I(r) \frac{d\Phi_{II}}{dr}(r) - \Phi_{II}(r) \frac{d\Phi_I}{dr}(r), \tag{49}$$

vanishes at an arbitrary radius r between zero and r_b , and hence at all radii.⁶³ $\text{Wk}=0$ indicates that ω is an eigenfrequency, and $\Phi_I (\propto \Phi_{II})$ is an eigenfunction. The values of ε and r_b are decreased and increased, respectively, until the eigenfrequency converges to the desired accuracy.

C. Dominant modes

We now examine the dominant modes of a smoothed Rankine cyclone, with parameters $\Delta=0.025$, $l_2=r_0$, and

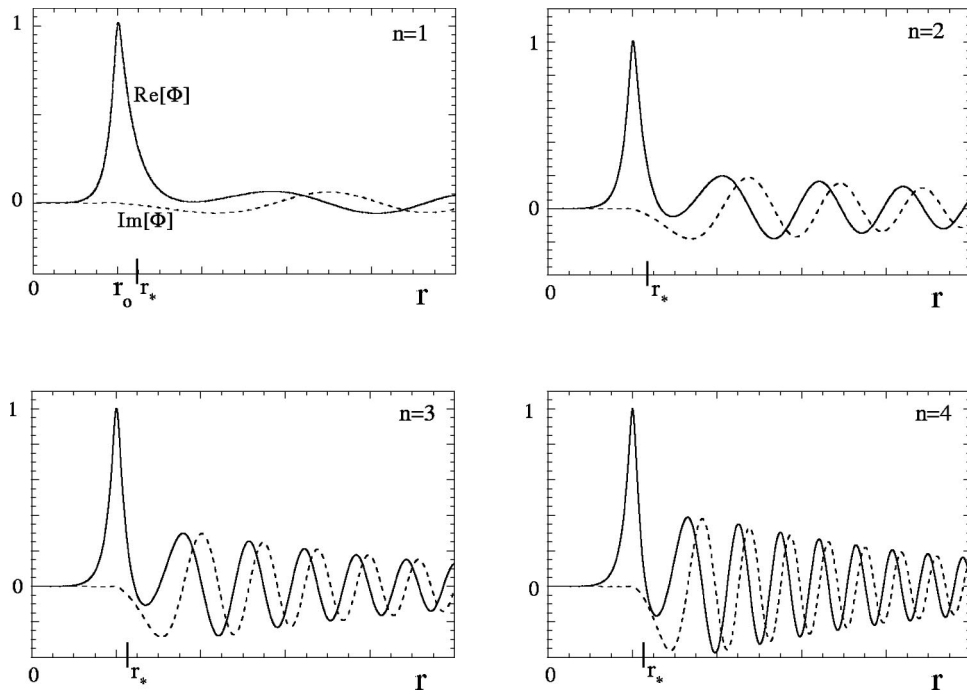


FIG. 5. Geopotential eigenfunctions for the $m=2$ dominant modes of a smoothed Rankine cyclone. The cyclone parameters are $Ro=10$, $l_2=r_0$, and $\Delta=0.025$. The $n=2$ dominant mode was shown previously, in Fig. 3(a).

$Ro=10$. By definition, a *dominant mode* is the fastest growing eigenmode for a given wave vector (m,n) .

Figure 5 shows the geopotential perturbation $\Phi(r)$ for several dominant modes. Each mode has the same vertical wave number, $m=2$. The azimuthal wave numbers vary from $n=1$ to $n=4$. Extended tick marks indicate the locations of the critical radii. In each case, r_* is greater than r_0 .

Figure 6 shows the complex frequency $\omega = \omega_R + i\omega_I$ of the dominant mode for each n , as m increases from 0 to 4. The shortest e -folding time (ω_I^{-1}) in this sample is about four central rotation periods. The $m=0$ frequencies were calculated analytically, assuming a radially unbounded

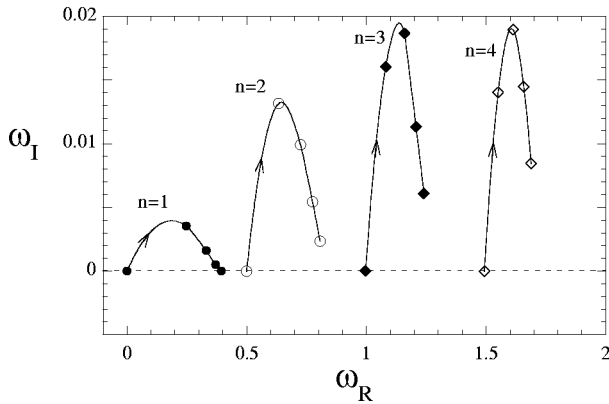


FIG. 6. Complex frequencies of the dominant modes of a smoothed Rankine cyclone. ω_I is the growth rate and ω_R is the oscillation frequency. Solid curves connect the data for a single azimuthal wave number n . Arrows are in the direction of increasing vertical wave number, $m \in \{0,1,2,3,4\}$. The cyclone parameters are $Ro=10$, $l_2=r_0$, and $\Delta=0.025$. ω_I and ω_R are normalized to the central vorticity Z_0 .

domain.^{14,18} These modes are stable because they represent pure VR waves.

We may view each dominant mode as having inner and outer parts. As in Sec. I, we identify the inner part as a VR wave. It is peaked approximately where $|d\bar{q}/dr|$ is maximum, and is retrograde ($\omega_R/n < \bar{\Omega}$) at that location. As the radius r increases, the mean cyclonic flow becomes negligible. In this outer region, the eigenmode is a spiral wave that propagates away from the vortex. There is no local PV gradient to support this propagation. Accordingly, we identify the outer part of the dominant mode as an IB wave.

We note that a shooting code does not necessarily find the dominant mode. However, we have checked (for many cases) that the modes in Figs. 5–7 dominate numerical integrations of the initial value problem, after short transition periods. Our numerical simulations employed a sponge-ring boundary condition, with absorption coefficient $D=20$, and $r_w=7.5r_0$ (see Appendix D). The initial conditions were simple vortex deformations as in Ref. 20.

V. STABILIZATION OF A SMOOTHED RANKINE CYCLONE: A HINT OF CRITICAL LAYER DAMPING

Figure 7 illustrates how smoothing the edge of the vortex (increasing Δ) decreases the growth rate ω_I of a dominant mode. It is crucial to realize that smoothing the edge actually *steepens* the unperturbed PV profile at the critical radius r_* . As a result, CL damping intensifies. This would explain the observed decay of ω_I .

As Δ surpasses a threshold, ω_I becomes negative. As ω_I becomes negative, the wave becomes a *quasimode*.^{8,9,14–20} Over most of the cyclone, a quasimode behaves like a single damped wave. In contrast, the PV perturbation grows in the

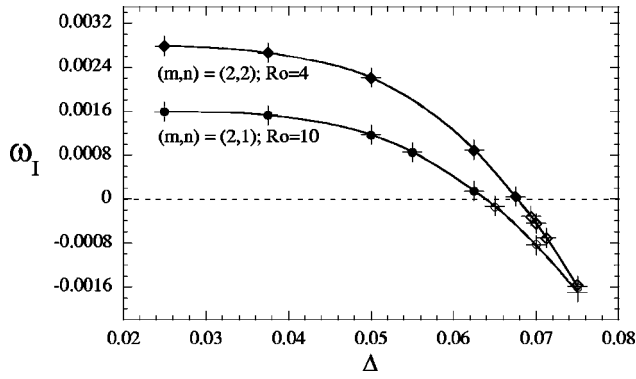


FIG. 7. Growth rate of two VR waves as a function of the smoothness parameter Δ . Increasing Δ corresponds to increasing the PV gradient at the critical radius r_* . Filled or empty symbols indicate that the VR wave is a normal mode or quasimode, respectively. The cross-hairs correspond to Eq. (70). The solid curves are to aid the eye. The fixed cyclone parameter is $l_2 = r_0$. ω_1 is normalized to Z_0 .

critical layer. Consequently, the disturbance is not a solution to the eigenmode problem. Appendix E describes a method for computing the complex frequencies of quasimodes. The resulting values for ω_1 appear as empty symbols in Fig. 7.

The data in Fig. 6 also reflect the stabilizing influence of a steepened PV profile at r_* . As the vertical wave number m increases, the critical radius decreases to a region of larger $d\bar{q}/dr$.^{9,20} Accordingly, ω_1 eventually diminishes.

VI. CRITICAL LAYER DAMPING VERSUS IB WAVE EMISSION

Figure 8 illustrates the interaction of a VR wave with its critical layer and the environment. A VR wave acts on the environment by emitting an IB wave. It acts on the critical layer by resonantly disturbing PV in that region. The results of Sec. IV indicated that IB wave emission has positive feedback.^{24–30} The results of Sec. V indicated that PV stirring in the critical layer has negative feedback.^{9,14–20} In what follows, we will use conservation of wave activity to quantify the competition between both feedbacks.

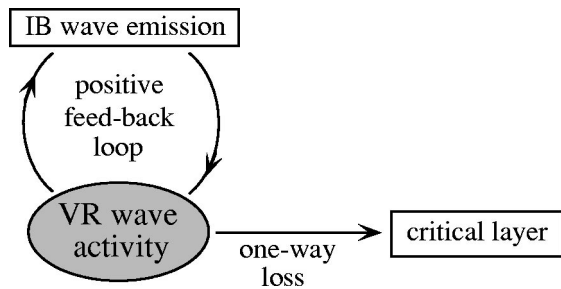


FIG. 8. Diagram showing the source and sink of VR wave activity (amplitude), according to linearized dynamics.

A. Decomposition of wave activity

We assume that the perturbation within the cyclone is dominated by a single VR wave, with a critical radius at r_* . Furthermore, we divide the wave activity into bulk (b) and critical layer (cl) components:

$$A_v(t; r_v) = A_b(t; r_v, r_*) + A_{cl}(t; r_*), \tag{50}$$

in which

$$A_b \equiv - \int_0^{2\pi} \int_0^H \int_0^{r_v} (d\varphi dz dr) \mathcal{L}_p, \tag{51}$$

and

$$A_{cl} \equiv - \int_0^{2\pi} \int_0^H \int_{r_* - \delta r}^{r_* + \delta r} (d\varphi dz dr) \mathcal{L}_p. \tag{52}$$

Here, δr is the half width of the critical layer, and \int denotes integration outside the critical layer, i.e., over the bulk of the vortex. Ultimately, we will consider the limit $\delta r \rightarrow 0^+$. With the present decomposition, conservation of wave activity [Eq. (35)] becomes

$$\frac{d}{dt} A_b = S_{rad} - \frac{d}{dt} A_{cl}. \tag{53}$$

In principle, the vortex radius r_v is arbitrary, insofar as it is greater than $r_* + \delta r$. Choosing r_v near its lower limit typically ensures that A_b represents the VR wave activity, with only a small contribution from the emitted IB wave.

B. Growth rate formula: A physical derivation

In this subsection, we derive an analytical expression for the growth rate of a VR wave. Our presentation aims to elucidate the dynamics, at the expense of mathematical rigor. Appendix F outlines a more formal derivation.

Because a single wave dominates the perturbation, we may write

$$\begin{aligned} \phi'(r, \varphi, z, t) &\approx a(t) \Phi(r) \cos(m\pi z/H) e^{i(n\varphi - \omega_R t)} + c.c., \\ u'(r, \varphi, z, t) &\approx a(t) U(r) \cos(m\pi z/H) e^{i(n\varphi - \omega_R t)} + c.c., \\ v'(r, \varphi, z, t) &\approx a(t) V(r) \cos(m\pi z/H) e^{i(n\varphi - \omega_R t)} + c.c., \\ w'(r, \varphi, z, t) &\approx a(t) W(r) \sin(m\pi z/H) e^{i(n\varphi - \omega_R t)} + c.c. \end{aligned} \tag{54}$$

Here, as opposed to (38), the frequency ω_R in the exponential is real, and the amplitude a is a complex valued function of time. In the critical layer, we permit a small correction to the single wave model. To emphasize its potential deviance, we separate the critical layer disturbance from the bulk disturbance. For example, the PV perturbation becomes

$$q'(r, \varphi, z, t) = \begin{cases} a(t)Q(r)\cos(m\pi z/H)e^{i(n\varphi - \omega_R t)} + \text{c.c.} & |r - r_*| > \delta r \\ \hat{q}_{\text{cl}}(r, t)\cos(m\pi z/H)e^{in\varphi} + \text{c.c.} & |r - r_*| < \delta r \end{cases} \quad (55)$$

In the single wave model, dA_b/dt is proportional to the rate of change of $|a|$. In particular,

$$\frac{d}{dt}A_b = M|a| \frac{d|a|}{dt}. \quad (56)$$

Here, we have introduced the weight

$$M \equiv \int_0^{r_v} dr [\alpha_1(r) + \alpha_2(r)], \quad (57)$$

in which

$$\alpha_1(r) \equiv -\frac{2\pi Hg}{\theta_0 N^2} r^2 \frac{|Q|^2}{d\bar{q}/dr}, \quad (58)$$

and

$$\alpha_2(r) \equiv -\frac{4\pi H}{f^2 l_m^2} r^2 \mathcal{R}[V\Phi^*]. \quad (59)$$

In Eq. (59), $\mathcal{R}[\dots]$ denotes the real part of the quantity in square brackets.

We may also relate S_{rad} and dA_{cl}/dt to the wave amplitude $|a|$. Substituting the single wave solution into the right-hand-side of Eq. (36) yields

$$S_{\text{rad}} = \epsilon_{\text{rad}}|a|^2, \quad (60)$$

in which

$$\epsilon_{\text{rad}} \equiv 2\pi H r_v^2 \mathcal{R}[UV^*]_{r_v}. \quad (61)$$

Substituting a generic critical layer perturbation into the definition of A_{cl} , and taking the time derivative, yields

$$\begin{aligned} \frac{d}{dt}A_{\text{cl}} &= -\frac{\pi Hg}{\theta_0 N^2} \int_{r_* - \delta r}^{r_* + \delta r} dr \frac{r^2}{d\bar{q}/dr} \partial_t(\hat{q}_{\text{cl}}\hat{q}_{\text{cl}}^*) \\ &\quad - \frac{\pi H}{f^2 l_m^2} \int_{r_* - \delta r}^{r_* + \delta r} dr r^2 \partial_t(\hat{v}_{\text{cl}}\hat{\phi}_{\text{cl}}^* + \text{c.c.}). \end{aligned} \quad (62)$$

In the critical layer, the linearized PV equation (29) takes the form

$$\partial_t \hat{q}_{\text{cl}} + in\bar{\Omega} \hat{q}_{\text{cl}} = -aUe^{-i\omega_R t} \frac{d\bar{q}}{dr}. \quad (63)$$

Here, we have approximated u' by its dominant single wave component, since it is multiplied by a small parameter ($d\bar{q}/dr$ near r_*). Integrating Eq. (63) yields

$$\hat{q}_{\text{cl}} = -U \frac{d\bar{q}}{dr} e^{-in\bar{\Omega}t} \int_0^t dt' a(t') e^{i(n\bar{\Omega} - \omega_R)t'}, \quad (64)$$

provided that $\hat{q}_{\text{cl}} = 0$ at $t = 0$. Other initial conditions lead to the same growth rate formula (70).

Equation (64) implies that

$$\begin{aligned} \partial_t(\hat{q}_{\text{cl}}\hat{q}_{\text{cl}}^*) &= 2|U|^2 \left(\frac{d\bar{q}}{dr} \right)^2 \mathcal{R} \left[a(t) \int_0^t dt' a^*(t') \right. \\ &\quad \left. \times e^{i(n\bar{\Omega} - \omega_R)(t-t')} \right]. \end{aligned} \quad (65)$$

For $t \ll |a|/(d|a|/dt)$, we may substitute the approximation $a^*(t') \approx a^*(t)$ into the right-hand-side of Eq. (65). With some additional reduction, we find that the PV perturbation develops a sharp peak at the critical radius, i.e.,

$$\begin{aligned} \partial_t(\hat{q}_{\text{cl}}\hat{q}_{\text{cl}}^*) &\approx 2|U|^2 \left(\frac{d\bar{q}}{dr} \right)^2 \frac{\sin[(n\bar{\Omega} - \omega_R)t]}{n\bar{\Omega} - \omega_R} |a|^2(t) \\ &\approx 2\pi|U|^2 \left(\frac{d\bar{q}}{dr} \right)^2 \frac{\delta(r - r_*)}{n|d\bar{\Omega}/dr|} |a|^2(t), \end{aligned} \quad (66)$$

in which δ is the Dirac distribution. The second approximation is valid for $t \gg \omega_R^{-1}$.

A Frobenius analysis (Appendix C) of normal modes suggests that $\partial_t(\hat{v}_{\text{cl}}\hat{\phi}_{\text{cl}}^*)$ is at worst logarithmically singular near the critical radius r_* . Accordingly, the second term in Eq. (62) vanishes as the critical layer becomes infinitesimally thin.

Substituting Eq. (66) into (62), and taking the limit $\delta r \rightarrow 0^+$, yields

$$\frac{d}{dt}A_{\text{cl}} = \epsilon_{\text{cl}}|a|^2, \quad (67)$$

in which

$$\epsilon_{\text{cl}} \equiv -\frac{2\pi^2 Hg}{\theta_0 N^2} \left[\frac{r^2 |U|^2 d\bar{q}/dr}{n|d\bar{\Omega}/dr|} \right]_{r_*}. \quad (68)$$

Using Eqs. (56), (60), and (67), we may convert conservation of wave activity (53) into an amplitude equation

$$M \frac{d|a|}{dt} = (\epsilon_{\text{rad}} - \epsilon_{\text{cl}})|a|. \quad (69)$$

The solution to Eq. (69) is $|a| = a_0 e^{\omega_1 t}$, where

$$\omega_1 = \frac{\epsilon_{\text{rad}} - \epsilon_{\text{cl}}}{M}, \quad (70)$$

and a_0 is a constant coefficient (cf. Ref. 50).

For all cases considered here, the weight M of the VR wave is positive. As a result, the sign of $\epsilon_{\text{rad}} - \epsilon_{\text{cl}}$ gives the sign of ω_1 . Assuming that $d\bar{q}/dr$ is negative at r_* , ϵ_{cl} is positive. Therefore, stirring of PV in the critical layer damps the VR wave. Assuming that the IB wave component of the mode transports angular momentum outward at the boundary, ϵ_{rad} is positive. Therefore, IB wave emission induces the

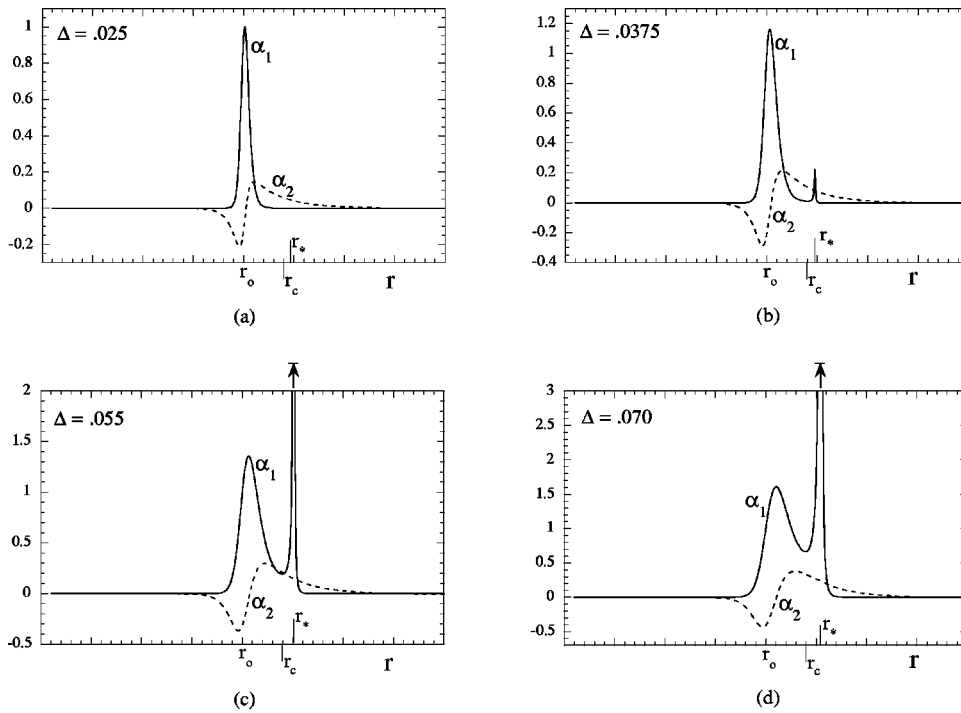


FIG. 9. Wave activity densities for the $(m,n)=(2,1)$ dominant mode of a smoothed Rankine cyclone, with fixed parameters $Ro=10$, $l_2=r_0$, and variable Δ as indicated. (d) corresponds to a damped quasimode. In a given plot, α_1 and α_2 have the same arbitrary units.

bulk wave to grow. This competition between PV stirring in the critical layer and IB wave emission was discussed earlier, in connection to Fig. 8.

We emphasize that the analysis leading to Eq. (69) requires that the amplitude of the wave grows or decays on a slower time scale than its oscillation period, i.e.,

$$\frac{\omega_I}{\omega_R} \ll 1. \tag{71}$$

That is, the wave must be near marginal stability.

C. Verification

We now verify the growth rate formula [Eq. (70)] of the previous subsection. In particular, we consider the normal modes of Fig. 7, which meet the requirement of weak growth

$$\frac{\omega_I}{\omega_R} < 5 \times 10^{-3} \ll 1. \tag{72}$$

To evaluate the growth rate formula, we must extract values for M , ϵ_{rad} , and ϵ_{cl} from the critical radius r_* and wave form $\Phi(r)$ of a computed mode. For ϵ_{rad} and ϵ_{cl} , the procedure is straightforward. The procedure for M requires further explanation.

Figure 9 plots the primary and secondary densities of the wave activity, $\alpha_1(r)$ and $\alpha_2(r)$, for four of the modes. Figure 9(a) corresponds to the case in which the smoothness parameter of the cyclone is smallest, i.e., $\Delta=0.025$. In this example, the PV gradient at the critical radius r_* is negligible, and α_1 has no visible amplitude there. Rather, α_1 is concentrated near r_0 , where the PV gradient is maximal. The secondary density α_2 extends over a broader region. Figures 9(b) and 9(c) correspond to cases in which $\Delta=0.0375$ and $\Delta=0.055$. For both modes, α_1 has a notable spike at the critical radius, where resonant stirring now acts on a larger

PV gradient. By definition, the integral M excludes this critical layer contribution. Accordingly, we make the approximation

$$M \approx \int_0^{r_c} dr \alpha_1(r) + \int_0^{r_v} dr \alpha_2(r), \tag{73}$$

in which r_c is between the spike of α_1 at r_* and the core region in which α_1 is otherwise concentrated. For all cases considered, we specifically set $r_c=1.2r_0$.

For quasimodes ($\omega_I < 0$) there is a more subtle issue (see Appendix E). Here the eigenvalue problem [Eq. (39)] is solved along a contour of the form

$$r = r_R + ir_1(r_R), \tag{74}$$

in which $0 \leq r_R \leq r_b$. The imaginary part r_1 satisfies $r_1(0) = 0 = r_1(r_b)$. In addition, the contour must arc above the complex critical radius. By choice, we keep r_1 uniformly positive and small, such that

$$0 \leq r_1 < 0.015r_0. \tag{75}$$

The eigenfunction $\Phi(r_R)$ that emerges from this problem only approximates the form of the physical quasimode. Nonetheless, it is used here to evaluate the analytical growth rate [Eq. (70)]. The procedure for quasimodes and normal modes is otherwise equivalent. Figure 9(d) plots the primary and secondary densities of modal wave activity, from which we calculate M , for a quasimode in a cyclone with $\Delta=0.07$. Note that by smoothing the cyclone, the distinction between the critical layer and bulk wave activity has become less obvious; yet, we have kept the separation at $r_c=1.2r_0$.

The cross-hairs (+) in Fig. 7 correspond to ω_I , given by Eq. (70), as explained. Apparently, Eq. (70) correctly describes the competition between CL damping and IB wave emission.

VII. CONCLUDING REMARKS

This paper has merged two disparate theories of discrete VR waves in a monotonic cyclone. One theory examined the decay of a VR wave due to the resonant disturbance of a PV gradient in its critical layer.^{9,14,16–20} Another theory examined the growth of a VR wave due to its excitation of a spiral IB wave in the ambient fluid.^{24–27} We have referred to these processes as *CL damping* and *IB wave emission*, respectively. CL damping was previously studied in the context of balance models, which ignore the influence of IB waves. IB wave emission was previously studied for the case of zero PV gradient in the critical layer.

We believe that Eq. (70) is the first analytical expression for the growth rate of a VR wave that includes *both* CL damping and IB wave emission.⁶⁴ This formula was derived as a corollary to conservation of wave activity (53). It shows that the wave will damp (or grow) if the PV gradient is above (or below) a threshold at the critical radius r_* .

Several past studies have shown that monotonic vortices that coarsely represent tropical cyclones are stable and will symmetrize.^{42,65,66} Furthermore, there is evidence that balance models adequately describe the linear dynamics of VR waves in such vortices, despite Rossby numbers of order 10–100.^{20,42} In part, this is because the CL damping of VR waves dominates the positive feedback of IB wave emission, i.e., $\epsilon_{cl}/\epsilon_{rad} \gg 1$.

Of course, even if balance models describe damped VR waves, they cannot describe the emitted IB waves. Further study of this transient radiation, in the context of the primitive equations, may provide insight into various weather patterns that emerge in and around tropical cyclones.⁶⁷ Here, we have focused on radiation from discrete VR waves. As mentioned earlier, discrete VR waves typically dominate vortex deformations. However, an arbitrary PV perturbation may also generate VR waves of another kind—sheared spirals.^{2–4,23,34–42} A comprehensive study would consider IB wave emission from both discrete and sheared VR waves.

ACKNOWLEDGMENTS

D.A.S. thanks Professor B. F. Farrell for a helpful discussion regarding the radial boundary conditions, which motivated Appendix D. He also thanks the Department of Earth and Planetary Sciences at Harvard University, for supporting this research through a Reginald Daly postdoctoral fellowship. Additional funding was provided by the National Science Foundation, through Grant No. ATM-0132006.

APPENDIX A: ISOMORPHISM BETWEEN ATMOSPHERIC AND OCEANIC DYNAMICS

It is worth mentioning that Eqs. (4)–(6), (9) are isomorphic with the following inviscid, hydrostatic, Boussinesq equations that can be used to model oceanic flow:¹¹

$$\partial_t \mathbf{u} + \mathbf{v} \cdot \nabla \mathbf{u} + f \hat{z} \times \mathbf{u} + \nabla_h \bar{p} = 0, \quad (\text{A1})$$

$$-\bar{p} = \partial_z \bar{p} / g, \quad (\text{A2})$$

$$\partial_t \bar{p} + \mathbf{v} \cdot \nabla \bar{p} = 0, \quad (\text{A3})$$

$$\nabla \cdot \mathbf{v} = 0. \quad (\text{A4})$$

Here, \bar{p} and $\bar{\rho}$ are pressure and mass density, both divided by the constant reference density ρ_0 . Equations (A1)–(A4) are obtained from (4)–(6), (9) by the transformation $\theta \rightarrow -\bar{p}$, $\phi \rightarrow \bar{p}$ and $g/\theta_0 \rightarrow g$. In addition, z has returned to actual height.

APPENDIX B: ANGULAR PSEUDOMOMENTUM

The angular pseudomomentum density is a function of the form

$$\mathcal{L}_p \equiv [\mathcal{L}(r, v) + C(q, \theta)] - [\mathcal{L}(r, \bar{v}) + C(\bar{q}, \bar{\theta})] - \nabla \cdot \mathbf{G}. \quad (\text{B1})$$

It is closely related to the vertical angular momentum density of the perturbation, $\mathcal{L}(r, v) - \mathcal{L}(r, \bar{v})$, and is flux conservative by construction. The Casimir function C and gauge vector \mathbf{G} are chosen so that \mathcal{L}_p is quadratic to lowest order in the perturbation fields.

We will attempt a solution for C and \mathbf{G} , assuming that C depends only on q . Then, a Taylor expansion of the first term in \mathcal{L}_p , about the cyclonic equilibrium, yields

$$\mathcal{L}_p \approx rvv' + \frac{dC}{dq} \bigg|_{\bar{q}} q' + \frac{1}{2} \frac{d^2C}{dq^2} \bigg|_{\bar{q}} (q')^2 - \nabla \cdot \mathbf{G} + O[(q')^3]. \quad (\text{B2})$$

We next substitute the relation

$$q' = \nabla \times \mathbf{u}' \cdot \hat{z} \frac{d\bar{\theta}}{dz} + \bar{\eta} \hat{z} \cdot \nabla \theta' + \nabla \cdot (\theta' \nabla \times \mathbf{u}') \quad (\text{B3})$$

into the second term on the right-hand side of Eq. (B2). To simplify the notation, let

$$c_1 \equiv r - \frac{d\bar{\theta}}{dz} \frac{d}{dr} \left(\frac{dC}{dq} \bigg|_{\bar{q}} \right), \quad (\text{B4})$$

$$\mathbf{c}_2 \equiv \frac{dC}{dq} \bigg|_{\bar{q}} \left[\hat{r} \frac{d\bar{\theta}}{dz} v' - \hat{\phi} \frac{d\bar{\theta}}{dz} u' + \hat{z} \bar{\eta} \theta' \right], \quad (\text{B5})$$

and

$$\mathbf{c}_3 \equiv \theta' \nabla \times \mathbf{u}'. \quad (\text{B6})$$

Then, Eq. (B2) becomes

$$\mathcal{L}_p \approx c_1 v' + \frac{dC}{dq} \bigg|_{\bar{q}} \nabla \cdot \mathbf{c}_3 + \frac{1}{2} \frac{d^2C}{dq^2} \bigg|_{\bar{q}} (q')^2 + \nabla \cdot (\mathbf{c}_2 - \mathbf{G}) + O[(q')^3]. \quad (\text{B7})$$

We may eliminate the first term on the right-hand side of Eq. (B7) by setting $c_1 = 0$. This condition is satisfied if

$$C(q) = \frac{g}{2\theta_0 N^2} \int_{q_{\max}}^q d\bar{q} R^2(\bar{q}), \quad (\text{B8})$$

in which $R(q)$ is the inverse of the mapping $q = \bar{q}(R)$, and q_{\max} is the maximum PV in the vortex. We have assumed that \bar{q} is monotonic. We have also recalled that $d\bar{\theta}/dz = \theta_0 N^2/g$. From Eq. (B8), we obtain

$$\frac{dC}{dq} \Big|_{\bar{q}} = \frac{g}{2\theta_0 N^2} r^2, \tag{B9}$$

and

$$\frac{d^2C}{dq^2} \Big|_{\bar{q}} = \frac{g}{\theta_0 N^2} \frac{r}{d\bar{q}/dr}. \tag{B10}$$

Furthermore,

$$\frac{dC}{dq} \Big|_{\bar{q}} \nabla \cdot \mathbf{c}_3 = \nabla \cdot \frac{gr^2}{2\theta_0 N^2} \mathbf{c}_3 + \frac{r}{N^2} \partial_z v' \partial_z \phi'. \tag{B11}$$

Substituting Eqs. (B9)–(B11) into Eq. (B7), and setting

$$\mathbf{G} = \mathbf{c}_2 + \frac{gr^2}{2\theta_0 N^2} \mathbf{c}_3, \tag{B12}$$

yields

$$\mathcal{L}_p = \frac{g}{2\theta_0 N^2} \frac{r(q')^2}{d\bar{q}/dr} + \frac{r}{N^2} \partial_z v' \partial_z \phi' + O[(q')^3]. \tag{B13}$$

So, we have arrived at a flux-conserved quantity, \mathcal{L}_p , that reduces to the right-hand side of Eq. (32) to lowest order in the perturbation fields. Its exact form is given below (cf. Ref. 59):

$$\mathcal{L}_p = rv' + \frac{g}{2\theta_0 N^2} \int_{\bar{q}}^q d\bar{q} R^2(\bar{q}) - \nabla \cdot \mathbf{G}. \tag{B14}$$

APPENDIX C: BEHAVIOR OF A MODE NEAR RESONANCES

This appendix briefly describes the form of $\Phi(r)$, and its derivatives, near the false and genuine singular points of the eigenmode equation (39). The false singular points are the inertial resonances, r_{\pm} , defined by

$$\sigma(r_{\pm}) \equiv \pm \sqrt{\bar{\mu}(r_{\pm})}. \tag{C1}$$

The genuine singular point is the complex critical radius r_s , defined by

$$\sigma(r_s) \equiv 0. \tag{C2}$$

A standard Frobenius analysis near r_{\pm} yields

$$\Phi(r_{\pm} + \varepsilon) = \Phi(r_{\pm}) \left[1 + \frac{n\bar{\xi}}{\sigma r} \Big|_{r_{\pm}} \varepsilon + O(\varepsilon^2) \right], \tag{C3}$$

in which $\varepsilon \equiv (r - r_{\pm})$. So, Φ is regular at the inertial resonances. A standard Frobenius analysis near r_s yields

$$\Phi(r_s + \varepsilon) = \Phi(r_s) \left[1 + \frac{\bar{\xi}}{\bar{\eta} r} \frac{d\bar{\xi}/dr}{d\bar{\Omega}/dr} \Big|_{r_s} \varepsilon \ln(\varepsilon) + O(\varepsilon) \right], \tag{C4}$$

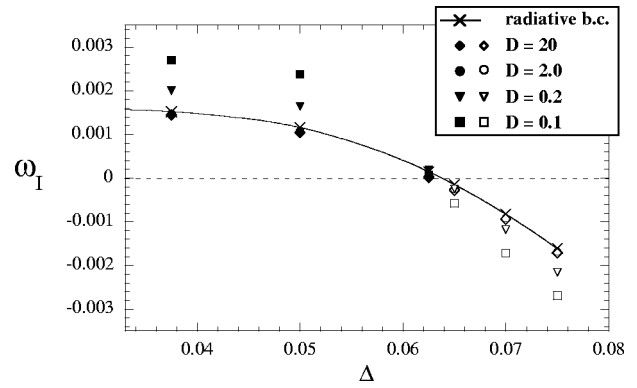


FIG. 10. Sponge-ring vs radiative boundary conditions. This plot shows the growth rate ω_1 of the $(m,n)=(2,1)$ dominant mode of a smoothed Rankine cyclone, with variable Δ . The cyclone parameters are $Ro=10$ and $l_2=r_0$. The \times markers, connected by a solid curve, correspond to a radiative boundary condition. The circles, triangles, diamonds, and squares correspond to sponge-ring boundary conditions, of varying absorption D , as indicated. Filled and empty symbols signify normal modes and quasimodes, respectively. ω_1 is normalized to Z_0 .

in which $\varepsilon \equiv (r - r_s)$. Therefore, in general, the first derivative of Φ is weakly (logarithmically) singular at the complex critical radius.

Equations (43) relate Φ to the velocity and PV perturbations. There are several results worth noting. One may verify, by direct substitution, that the velocity and PV perturbations are regular at the inertial resonances, r_{\pm} . At the complex critical radius r_s , U and W are continuous well-defined functions. On the other hand, V is logarithmically singular, and Q has a pole.

APPENDIX D: SPONGE-RING BOUNDARY CONDITION

Another notable treatment of the far-field radial boundary is to let a *sponge-ring* buffer a “wall” at $r=r_w$. Here, we apply a sponge ring that linearly damps the perturbation fields (u' , v' and $\partial_z \phi'$) at a rate

$$\gamma(r) = D \frac{\bar{\xi}(0)}{2} \left[1 + \tanh\left(\frac{15(r-r_w)}{2r_w}\right) \right], \tag{D1}$$

in which $D > 0$ is an adjustable absorption coefficient. Note that γ is effectively zero for $r \lesssim r_w(1 - 2/15)$. At the “wall,” we set

$$\Phi(r_w) = 0. \tag{D2}$$

A sponge ring slightly modifies the vortex eigenmode problem. To begin with, we must let

$$\sigma \rightarrow \omega - n\bar{\Omega} + i\gamma \tag{D3}$$

in Eq. (39). Furthermore, we must replace the radiative boundary condition (48) ($j=1$) with (D2).

Although a sponge ring is meant to absorb, it may partially reflect outward propagating IB waves. The value of D affects the reflectivity. In what follows, we examine how changing D varies the growth rate of a mode that represents the VR–IB wave instability.

Figure 10 shows the growth rate of the $(m,n)=(2,1)$

dominant mode of a smoothed Rankine cyclone [Eq. (37)], as a function of the parameter Δ . The fixed cyclone parameters are $Ro=10$ and $l_2=r_0$. The \times markers, connected by a solid curve, are the growth rates obtained by a radiative boundary condition at $r_b=5.5r_0$. The same data appear in Fig. 7.

The additional data result from sponge-ring boundaries (D1)–(D2), with $r_w=7.5r_0$. Filled symbols correspond to normal modes, whereas empty symbols correspond to quasimodes. For weak absorption ($D \leq 0.2$), the growth and decay rates differ notably from the solid curve. However, for $2 \leq D \leq 20$, the sponge-ring and radiative boundary conditions give approximately the same results.

Figure 10 merely illustrates the extent to which spongy and radiative boundary conditions can differ. A more comprehensive study is tangential, and not pursued here.

APPENDIX E: QUASIMODES

In this appendix, we briefly examine the formal definition of a quasimode, and present a method for computing its complex frequency.^{14,16,17} For simplicity, we consider a perturbation that consists of a single Fourier component, e.g., $\phi' = \hat{\phi}(r,t)\cos(m\pi z/H)e^{im\varphi} + c.c.$ We may define the Laplace transform of the Fourier coefficient $\hat{\phi}$, as follows:

$$\hat{\phi}_T(r, \nu) \equiv \int_0^\infty dt \hat{\phi}(r,t) e^{i\nu t}. \quad (\text{E1})$$

As such, the inversion contour is in the upper half of the complex ν plane, and is antiparallel to the real ν axis; i.e.,

$$\hat{\phi}(r,t) = -\frac{1}{2\pi} \int_{\infty+i\beta}^{-\infty+i\beta} d\nu \hat{\phi}_T(r,\nu) e^{-i\nu t}, \quad (\text{E2})$$

where $\beta > 0$.

By standard techniques, we may convert the linearized equations of motion into a single differential equation in r for $\hat{\phi}_T$. Following Ref. 14, we may solve this differential equation with the aid of a Green function.

For the purposes of this appendix, we need only consider the form of the solution at the boundary radius r_b :

$$\hat{\phi}_T(r_b, \nu) = \int_0^{r_b} dr r F(\nu, r) \Phi_I(r) \Phi_{II}(r_b) \frac{\bar{\mu}(r) - \sigma^2(r)}{r \text{Wk}(\nu, r)}. \quad (\text{E3})$$

Here, F is a function that depends on both the basic vortical flow and the initial perturbation. As before, Φ_I and Φ_{II} are independent solutions of Eq. (39), with end-point conditions (45) and (48) ($j=1$), respectively. Their ν dependence is implicit. Notably, the Wronskian of Φ_I and Φ_{II} [Eq. (49)] appears in the denominator of the integrand.

As a result, poles of $\hat{\phi}_T(r_b, \nu)$ will occur at discrete values of ν where the Wronskian is zero (for any and all r between 0 and r_b). Each pole explicitly contributes a term to $\hat{\phi}(r_b, t)$ that oscillates at a discrete frequency, and grows or decays exponentially with time. One zero of Wk , at $\nu = \omega$, corresponds to the dominant growing eigenmode of Sec. IV C. We will refer to this zero as the *dominant root*.

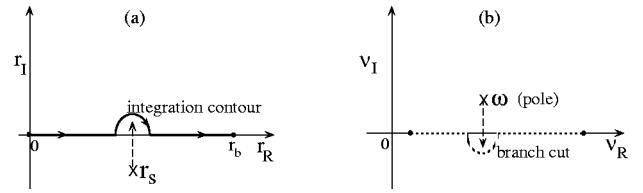


FIG. 11. As the PV gradient at r_* increases above a threshold: (a) the imaginary part of the complex critical radius r_s becomes positive and (b) the imaginary part of the mode frequency ω becomes negative. Such changes are indicated by the dashed arrows. Above the gradient threshold, one must deform the radial integration contour above r_s in order to keep ω as a pole in the analytic continuation of the geopotential transform $\hat{\phi}_T$. Otherwise, the pole will “slip underneath” the branch cut. The subscripts R and I denote the real and imaginary parts of the complex variables r and ν .

By analogy to the theory developed in Ref. 14, we may assume that Wk has a branch cut along the real ν axis. By further analogy, we may assume that the dominant root of Wk will “slip underneath” this branch cut, and disappear, as the magnitude of $d\bar{q}/dr$ increases above a threshold at r_* . However, the analytic properties of Wk vary with the radial contour r on which it is defined, i.e., the flexible integration contour in Eq. (E3). If we bend the radial contour above the real r axis [Fig. 11(a)], the branch cut of Wk will dip below the real ν axis [Fig. 11(b)]. The dominant root will reappear if the radial contour arches over the complex critical radius r_s , defined by $n\bar{\Omega}(r_s) = \omega$.

The recovered root of Wk , and pole of $\hat{\phi}_T$, corresponds to an exponentially damped quasimode. From above, we conclude that the procedures for computing eigenmode and quasimode frequencies hardly differ. To find an eigenfrequency, we solve the equation $\text{Wk}(\omega, r) = 0$ for ω , on the real r axis. To find a quasimode frequency, we must solve the equation $\text{Wk}(\omega, r) = 0$ for ω on a *deformed* radial contour, similar to that in Fig. 11(a). Our numerics (see Sec. IV B) was easily generalized for this task. The principal modification was to integrate Eq. (39) for Φ_I and Φ_{II} along the deformed radial contour.

APPENDIX F: ALTERNATIVE DERIVATION OF THE GROWTH RATE FORMULA

Assume that the perturbation is an exponentially growing mode. Substituting the normal mode solution [Eq. (38)] into conservation of wave activity [Eq. (35)] yields

$$\int_0^{r_b} dr \omega_1 (\alpha_1 + \alpha_2) = \epsilon_{\text{rad}}, \quad (\text{F1})$$

where α_1 , α_2 , and ϵ_{rad} were defined by Eqs. (58), (59), and (61). Using the identity

$$\omega_1 = \frac{i}{2} (\sigma_- - \sigma_+), \quad (\text{F2})$$

in which $\sigma_{\pm} \equiv \omega_R - n\bar{\Omega} \pm i\omega_1$, we may write

$$\omega_1 \alpha_1 = -\frac{i\pi Hg}{\theta_0 N^2} r^2 \frac{d\bar{q}}{dr} \left(\frac{|U|^2}{\sigma_+} - \frac{|U|^2}{\sigma_-} \right). \quad (\text{F3})$$

Note that we have used Eq. (43) to express α_1 as a function of U , rather than Q .

Consider the expansion

$$\int_0^{r_v} dr r^2 \frac{d\bar{q}}{dr} \frac{|U|^2}{\sigma_{\pm}} = \left[1 \pm i\omega_1 \frac{\partial}{\partial \omega_R} + \dots \right] \lim_{\omega_1 \rightarrow 0^+} \int_0^{r_v} dr r^2 \frac{d\bar{q}}{dr} \frac{|U|^2}{\sigma_{\pm}}. \tag{F4}$$

From the Plemelj formula⁶⁸

$$\lim_{\omega_1 \rightarrow 0^+} \int_0^{r_v} dr r^2 \frac{d\bar{q}}{dr} \frac{|U|^2}{\sigma_{\pm}} = \int_0^{r_v} dr r^2 \frac{d\bar{q}}{dr} \frac{|U|^2}{\omega_R - n\Omega} \mp i\pi \left[\frac{r^2 |U|^2 d\bar{q}/dr}{n |d\bar{\Omega}/dr|} \right]_{r_*}, \tag{F5}$$

where \int denotes the principal part, fractured at the critical radius r_* .

Suppose that $rd\bar{q}/dr$ is of order ω_1 (or less) for $r \geq r_c$, where $r_c < r_*$. Then, using Eqs. (F3)–(F5), we obtain

$$\int_0^{r_v} dr \omega_1 \alpha_1 = -\omega_1 \frac{2\pi Hg}{\theta_0 N^2} \int_0^{r_c} dr r^2 \frac{d\bar{q}}{dr} \frac{|U|^2}{(\omega_R - n\Omega)^2} - \frac{2\pi^2 Hg}{\theta_0 N^2} \left[\frac{r^2 |U|^2 d\bar{q}/dr}{n |d\bar{\Omega}/dr|} \right]_{r_*} + O(\omega_1^2). \tag{F6}$$

Further simplification yields

$$\int_0^{r_v} dr \omega_1 \alpha_1 = \omega_1 \int_0^{r_c} dr \alpha_1 + \epsilon_{cl} + O(\omega_1^2), \tag{F7}$$

in which ϵ_{cl} was defined by Eq. (68).

Substituting Eq. (F7) into (F1) reproduces the growth rate formula of the main text (70), with M given by (73).

¹J. C. McWilliams, J. B. Weiss, and I. Yavneh, "The vortices of homogeneous geostrophic turbulence," *J. Fluid Mech.* **401**, 1 (1999).
²J. Enagonio and M. T. Montgomery, "Tropical cyclogenesis via convectively forced Rossby waves in a shallow water primitive equation model," *J. Atmos. Sci.* **44**, 685 (2001).
³J. D. Moller and M. T. Montgomery, "Vortex Rossby waves and hurricane intensification in a barotropic model," *J. Atmos. Sci.* **56**, 1674 (1999).
⁴M. T. Montgomery and J. Enagonio, "Tropical cyclogenesis via convectively forced vortex rossby waves in a three-dimensional quasigeostrophic model," *J. Atmos. Sci.* **55**, 3176 (1998).
⁵L. M. Polvani, "Two-layer geostrophic vortex dynamics. Part 2: Alignment and two-layer V-states," *J. Fluid Mech.* **225**, 241 (1991).
⁶F. Viera, "On the alignment and axisymmetrization of a vertically tilted geostrophic vortex," *J. Fluid Mech.* **289**, 29 (1995).
⁷G. G. Sutyryn, J. C. McWilliams, and R. Saravanan, "Co-rotating stationary states and vertical alignment of geostrophic vortices with thin cores," *J. Fluid Mech.* **357**, 321 (1998).
⁸P. D. Reasor and M. T. Montgomery, "Three-dimensional alignment and co-rotation of weak, TC-like vortices via linear vortex-Rossby-waves," *J. Atmos. Sci.* **58**, 2306 (2001).
⁹D. A. Schecter, M. T. Montgomery, and P. D. Reasor, "A theory for the vertical alignment of a quasigeostrophic vortex," *J. Atmos. Sci.* **59**, 150 (2002).

¹⁰For a related discussion of 2D symmetrization, the reader may consult the following: M. V. Melander, J. C. McWilliams, and N. J. Zabusky, "Axisymmetrization and vorticity gradient intensification of an isolated two-dimensional vortex through filamentation," *J. Fluid Mech.* **178**, 137 (1987).
¹¹J. Pedlosky, *Geophysical Fluid Dynamics* (Springer, New York, 1987), Chap. 6.
¹²J. C. McWilliams, "A uniformly valid model spanning the regimes of geostrophic and isotropic, stratified turbulence: Balanced turbulence," *J. Atmos. Sci.* **42**, 1773 (1985).
¹³Vortex Rossby waves are analogous to planetary Rossby waves; however, they were first studied in a simplified context by Kelvin. See Lord Kelvin, "On the vibrations of a columnar vortex," *Philos. Mag.* **10**, 155 (1880).
¹⁴R. J. Briggs, J. D. Daugherty, and R. H. Levy, "Role of Landau damping in crossed-field electron beams and inviscid shear flow," *Phys. Fluids* **13**, 421 (1970).
¹⁵S. Pillai and R. W. Gould, "Damping and trapping in 2D inviscid fluids," *Phys. Rev. Lett.* **73**, 2849 (1994).
¹⁶N. R. Corngold, "Linear response of the two-dimensional pure electron plasma: Quasimodes for some model profiles," *Phys. Plasmas* **2**, 620 (1995).
¹⁷R. L. Spencer and S. N. Rasband, "Damped diocotron quasi-modes of nonneutral plasmas and inviscid fluids," *Phys. Plasmas* **4**, 53 (1997).
¹⁸D. A. Schecter, D. H. E. Dubin, A. C. Cass, C. F. Driscoll, I. M. Lansky, and T. M. O'Neil, "Inviscid damping of asymmetries on a two-dimensional vortex," *Phys. Fluids* **12**, 2397 (2000).
¹⁹N. J. Balmforth, S. G. Llewellyn Smith, and W. R. Young, "Disturbing vortices," *J. Fluid Mech.* **426**, 95 (2001).
²⁰D. A. Schecter and M. T. Montgomery, "On the symmetrization rate of an intense geophysical vortex," *Dyn. Atmos. Oceans* **37**, 55 (2003).
²¹L. J. Shapiro and M. T. Montgomery, "A three-dimensional balance theory for rapidly rotating vortices," *J. Atmos. Sci.* **50**, 3322 (1993).
²²S. Ren, "Further results on the stability of rapidly rotating vortices in the asymmetric balance formulation," *J. Atmos. Sci.* **56**, 475 (1999).
²³J. C. McWilliams, L. P. Graves, and M. T. Montgomery, "A formal theory for vortex Rossby waves and vortex evolution," *Geophys. Astrophys. Fluid Dyn.* **97**, 275 (2003).
²⁴R. Plougonven and V. Zeitlin, "Internal gravity wave emission from a pancake vortex: An example of wave-vortex interaction in strongly stratified flows," *Phys. Fluids* **14**, 1259 (2002).
²⁵R. Ford, "The instability of an axisymmetric vortex with monotonic potential vorticity in rotating shallow water," *J. Fluid Mech.* **280**, 303 (1994).
²⁶R. Ford, "The response of a rotating ellipse of uniform potential vorticity to gravity wave radiation," *Phys. Fluids* **6**, 3694 (1994).
²⁷K. C. Chow and K. L. Chan, "Angular momentum transports by moving spiral waves," *J. Atmos. Sci.* **60**, 2004 (2003).
²⁸R. Ford, M. E. McIntyre, and W. A. Norton, "Balance and the slow quasimanifold: Some explicit results," *J. Atmos. Sci.* **57**, 1236 (2000).
²⁹S. Saujani and T. G. Shepherd, "Comments on 'Balance and the slow quasimanifold: Some explicit results,'" *J. Atmos. Sci.* **59**, 2874 (2002).
³⁰R. Ford, M. E. McIntyre, and W. A. Norton, "Reply to Comment by S. Saujani and T. G. Shepherd on 'Balance and the slow quasimanifold: Some explicit results,'" *J. Atmos. Sci.* **59**, 2878 (2002).
³¹E. G. Broadbent and D. W. Moore, "Acoustic destabilization of vortices," *Philos. Trans. R. Soc. London, Ser. A* **290**, 353 (1979).
³²W. M. Chan, K. Shariff, and T. H. Pulliam, "Instabilities of two-dimensional inviscid compressible vortices," *J. Fluid Mech.* **253**, 173 (1993).
³³J. C. McWilliams, I. Yavneh, M. J. P. Cullen, and P. R. Gent, "The breakdown of large-scale flows in rotating, stratified fluids," *Phys. Fluids* **10**, 3178 (1998).
³⁴M. T. Montgomery and R. J. Kallenbach, "A theory of vortex Rossby-waves and its application to spiral bands and intensity changes in hurricanes," *Q. J. R. Meteorol. Soc.* **123**, 435 (1997).
³⁵A. P. Bassom and A. D. Gilbert, "The spiral wind-up of vorticity in an inviscid planar vortex," *J. Fluid Mech.* **371**, 109 (1998).
³⁶G. Brunet and M. T. Montgomery, "Vortex Rossby waves on smooth circular vortices: I. Theory," *Dyn. Atmos. Oceans* **35**, 153 (2002).
³⁷M. T. Montgomery and G. Brunet, "Vortex Rossby waves on smooth circular vortices: II. Idealized numerical experiments for tropical cyclone and polar vortex interiors," *Dyn. Atmos. Oceans* **35**, 179 (2002).
³⁸Y. Chen and M. K. Yau, "Spiral bands in a simulated hurricane. Part I: Vortex Rossby wave verification," *J. Atmos. Sci.* **58**, 2128 (2001).

- ³⁹Y. Chen, G. Brunet, and M. K. Tau, "Spiral bands in a simulated hurricane. Part II: Wave activity diagnostics," *J. Atmos. Sci.* **60**, 1239 (2003).
- ⁴⁰Y. Wang, "Vortex Rossby waves in a numerically simulated tropical cyclone. Part I: Overall structure, potential vorticity, and kinetic energy budgets," *J. Atmos. Sci.* **59**, 1213 (2002).
- ⁴¹Y. Wang, "Vortex Rossby waves in a numerically simulated tropical cyclone. Part II: The role in tropical cyclone structure and intensity changes," *J. Atmos. Sci.* **59**, 1239 (2002).
- ⁴²P. D. Reasor, M. T. Montgomery, and L. D. Grasso, "A new look at the problem of tropical cyclones in shear flow: Vortex resiliency," *J. Atmos. Sci.* (in press).
- ⁴³D. A. Schecter and M. T. Montgomery, "The symmetrization rate of a geophysical vortex: Extension of theory to large Rossby numbers," *Proceedings of the 14th Conference on Atmospheric and Oceanic Fluid Dynamics* (American Meteorological Society, San Antonio, TX, 2003), p. 48.
- ⁴⁴W. D. Smyth and J. C. McWilliams, "Instability of an axisymmetric vortex in a stably stratified rotating environment," *Theor. Comput. Fluid Dyn.* **11**, 305 (1998).
- ⁴⁵The eventual destabilizing effect of nonlinear critical layer stirring has been observed in other systems. See, for example, N. J. Balmforth and Y.-N. Young, "Stratified Kolmogorov flow," *J. Fluid Mech.* **450**, 131 (2002).
- ⁴⁶T. B. Mitchell and C. F. Driscoll, "Symmetrization of 2D vortices by beat-wave damping," *Phys. Rev. Lett.* **73**, 2196 (1994).
- ⁴⁷A. Kubokawa, "Instability of a geostrophic front and its energetics," *Geophys. Astrophys. Fluid Dyn.* **33**, 223 (1985).
- ⁴⁸N. J. Balmforth, "Shear instability in shallow water," *J. Fluid Mech.* **387**, 97 (1998).
- ⁴⁹E. S. Benilov, "Short-wave, localized disturbances in jets, with applications to flows on a beta plane with topography," *Phys. Fluids* **15**, 718 (2003).
- ⁵⁰J. C. B. Papaloizou and J. E. Pringle, "The dynamical stability of differentially rotating discs—III," *Mon. Not. R. Astron. Soc.* **225**, 267 (1987).
- ⁵¹J. C. B. Papaloizou and D. N. C. Lin, "Theory of accretion disks I: Angular momentum transport processes," *Annu. Rev. Astron. Astrophys.* **33**, 505 (1995).
- ⁵²I. G. Shukhman, "Nonlinear evolution of spiral density waves generated by the instability of the shear layer in a rotating compressible fluid," *J. Fluid Mech.* **233**, 587 (1990).
- ⁵³B. J. Hoskins and F. P. Bretherton, "Atmospheric frontogenesis models: Mathematical formulation and solution," *J. Atmos. Sci.* **29**, 11 (1972).
- ⁵⁴M. E. McIntyre, "On the 'wave-momentum' myth," *J. Fluid Mech.* **106**, 331 (1981).
- ⁵⁵I. M. Held, "Pseudomomentum and orthogonality of modes in shear flows," *J. Atmos. Sci.* **42**, 2280 (1985).
- ⁵⁶I. M. Held and P. J. Phillips, "Linear and nonlinear barotropic decay on the sphere," *J. Atmos. Sci.* **42**, 200 (1987).
- ⁵⁷M. E. McIntyre and T. G. Shepherd, "An exact local conservation theorem for finite amplitude disturbances to non-parallel shear-flows, with remarks on Hamiltonian structure and on Arnol'd's stability theorems," *J. Fluid Mech.* **181**, 527 (1987).
- ⁵⁸P. H. Haynes, "Forced, dissipative generalizations of finite amplitude wave-activity conservation relations for zonal and nonzonal basic flows," *J. Atmos. Sci.* **45**, 2352 (1988).
- ⁵⁹T. A. Guinn and W. H. Schubert, "Hurricane spiral bands," *J. Atmos. Sci.* **50**, 3380 (1993).
- ⁶⁰The minimum frequency of an environmental IB wave is the Coriolis parameter f (see Ref. 61). In general, the VR wave frequency satisfies $\omega_R \sim nZ_0$. Frequency matching can occur only if $\omega_R \geq f$. For a Rossby wave with n of order unity, this condition becomes $Ro \geq 1$.
- ⁶¹A. E. Gill, *Atmosphere-Ocean Dynamics* (Academic, San Diego, CA, 1982), p. 258.
- ⁶²M. T. Montgomery and L. J. Shapiro, "Generalized Charney–Stern and Fjortoft theorems for rapidly rotating vortices," *J. Atmos. Sci.* **52**, 1829 (1995).
- ⁶³G. Birkhoff and G. C. Rota, *Ordinary Differential Equations* (Wiley, New York, 1989), p. 44.
- ⁶⁴As noted in Sec. I, Papaloizou and Pringle (Ref. 50) derived an analogous formula for the growth rate of an accretion disk wave. Such waves are affected by both critical layer stirring and *acoustic* radiation.
- ⁶⁵M. T. Montgomery and C. Lu, "Free waves on barotropic vortices. I. Eigenmode structure," *J. Atmos. Sci.* **54**, 1868 (1997).
- ⁶⁶D. S. Nolan and M. T. Montgomery, "Nonhydrostatic, three-dimensional perturbations to balanced, hurricane-like vortices. Part I: Linearized formulation, stability and evolution," *J. Atmos. Sci.* **59**, 2989 (2002).
- ⁶⁷K. C. Chow, K. L. Chan, and A. K. H. Lau, "Generation of moving spiral bands in tropical cyclones," *J. Atmos. Sci.* **59**, 2930 (2002).
- ⁶⁸J. Mathews and R. L. Walker, *Mathematical Methods of Physics* (Addison-Wesley, Redwood City, CA, 1970), p. 481.